# Impact of Scattering on the Capacity, Diversity, and Propagation Range of Multiple-Antenna Channels

Ada S. Y. Poon, *Member, IEEE,* David N. C. Tse, *Member, IEEE,* and Robert W. Brodersen, *Fellow, IEEE*

*Abstract*— The impact of scattering condition and array configuration on performances are inseparable in early analyses of multiple-antenna systems. An array-independent scattering model is introduced where three basic scattering mechanisms are modeled. Performance results become more intrinsic property of the scattering channel itself. For linear arrays of length $L$ in an environment of total angle spread $|\Omega|$, the ergodic capacity is shown to increase linearly with $L|\Omega|$ for large arrays. When antenna arrays reduce to practical sizes, the capacity scaling depends on the SNR as well. This implies that the number of antennas used should also depend on the SNR. In terms of outage capacity, the trade-off between spatial multiplexing gain and diversity gain is shown to be very sensitive to the underlying scattering mechanisms. Finally, as $|\Omega|$ varies with the propagation range, the trade-off among multiplexing gain, diversity gain, and propagation range is studied.

*Index Terms*— Multiple antennas, multiple-input multiple-output (MIMO) systems, physical channel modeling, antenna theory, spatial multiplexing, diversity

## I. Introduction

Multiple-antenna systems improve performance by exploiting the scattering nature of physical environments. To fully utilize this channel resource, early results [1]–[10] incorporate physical parameters of scattering condition into the channel model and study their effects on performances. They focus on models where scattering is captured by the fading statistics across all pairs of antennas. For example, [1]–[4] model the correlation across all pairs of antennas as a Kronecker product; [5]–[9] model the fading statistics as a composition of array manifolds and a random matrix capturing the scattering environment; and [10] model the fading statistics as a composition of two i.i.d. random matrices. While the fading statistics depends on the scattering condition, it also depends on the array configuration. As a result, different array configurations will yield different conclusions even in the *same* channel. A better understanding of the impact of scattering by itself will give us insights into choosing the array configuration and developing simpler space-time processing algorithms.

Previous work [11] proposed to capture the scattering condition by the angular intervals subtended by clusters of scatterers (see Fig. 1), and study antenna arrays that are limited by their
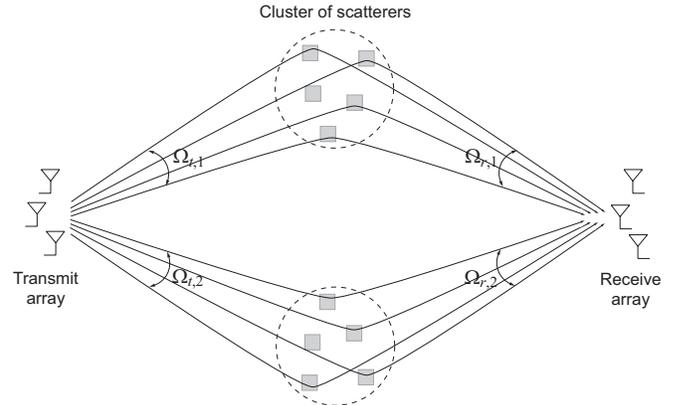
Fig. 1. Illustrates the angular interval subtended by clusters of scatterers at the transmitter $\Theta_t = \Theta_{t,1} \cup \Theta_{t,2} \cup \cdots$ and at the receiver $\Theta_r = \Theta_{r,1} \cup \Theta_{r,2} \cup \cdots$.

effective aperture but not the number of antennas. Performance results therefore do not depend on the array configuration. In [11], it demonstrates that the area constraint of antenna arrays and the angular intervals subtended by scatterers put forth a deterministic limit to the number of spatial degrees of freedom. For an array of effective aperture $\mathcal{A}$ in a physical environment of total angle spread $|\Omega|$ measured in solid angle, the number of spatial degrees of freedom is shown to be $\mathcal{A}|\Omega|$ for large $\mathcal{A}$. However, knowing the angular intervals of scatterers is not enough to characterize the impact of scattering on the channel capacity and diversity gain. To carry out such analyses, the joint response between the angular intervals at the transmitter and that at the receiver needs to be modeled.

The first part of this paper will supplement [11] with the joint response by modeling three basic scattering mechanisms: specular reflection, single-bounce diffuse scattering, and multi-bounce diffuse scattering (see Fig. 2). Based on the joint response, we will compute the channel capacity and diversity gain. [12] uses similar approach to model the antenna arrays but it uses the ray-tracing approach to model the scattering condition which lessens its analytical tractability. Our choice of the three scattering mechanisms is inspired by how they affect the path-loss exponent in the log-distance path-loss model [13]. The path-loss exponent reveals the dependence of the joint response between the transmit and the receive angular intervals: the larger the exponent is, the more diffuse the channel is, and the less dependence would be. The popular Kronecker model corresponds to the case of *no* dependence which is inconsistent with channel measurements [13] and pointed out by [14] as well.

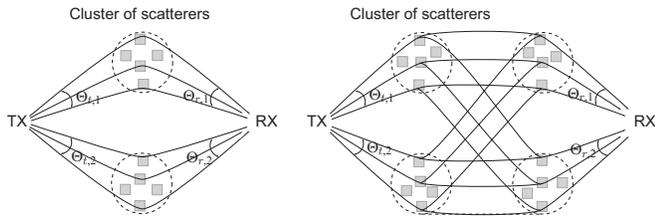We will first consider the fast fading channel and compute

Fig. 2. Illustrates (left) single-bounce diffuse scattering and (right) multi-bounce diffuse scattering.

the ergodic capacity for linear arrays of length $L$ normalized to a wavelength:

$$C = L|\Omega| \log(\gamma_1 \mathsf{SNR}) + o(L|\Omega|)$$

at high SNR where $|\Omega| := \int_\Theta \sin\theta \, d\theta$, $\Theta$ is the angular intervals subtended by scatterers and SNR is the transmit SNR. The gain $\gamma_1$ depends on the underlying scattering mechanisms. The capacity scaling factor is $L|\Omega|$ which is consistent with the previous work on the number of degrees of freedom for large arrays [11]. When $L|\Omega|$ is only a few times of wavelength which is often the case for practical uses of multiple-antenna systems, more terms in the capacity formula should be considered:

$$C = \Big[ L|\Omega| + \gamma_2 M \ln(L|\Omega|) \ln(\gamma_1 \mathsf{SNR}) \Big] \log(\gamma_1 \mathsf{SNR})$$
$$+ o\big(\ln(L|\Omega|)\big) \tag{1}$$

at high SNR where $M$ is the number of scattering clusters. The factor $\gamma_2$ depends on the underlying scattering mechanisms. The number of spatial degrees of freedom now depends on the SNR. This phenomenon is related to the concept of super-resolution and is more relevant to the spatial domain where practical $L|\Omega|$ is not large.

For the slow fading channel, we focus on the diversity gain and its trade-off with the spatial multiplexing gain (data rate). The diversity gain can differ by a factor of $M$ between single-bounce and multi-bounce diffuse scattering because there is more randomness in the latter than in the former. Thus, the difference between scattering mechanisms is more distinguishable in the slow fading scenario. Not only do the maximum diversity gains differ, the trade-offs between the spatial multiplexing gain and diversity gain in the outage formulation differ as well. We will follow the trade-off formulation in [15], and show that for a given multiplexing gain, the multi-bounce diffuse channel achieves an $M$-fold better diversity gain than the single-bounce diffuse channel in general. Since practical channels are more specular and single-bounce diffuse in nature as opposed to the Kronecker assumption, the insight obtained will help us design better space-time coding schemes.

Finally, as the scattering mechanisms studied are tied up with the path-loss model, the propagation range are therefore expected to relate to the multiplexing gain and diversity gain. We will illustrate that there is a trade-off between propagation range and multiplexing gain. As a whole, there is a range-multiplexing-diversity trade-off in the slow fading channel.

The rest of the paper is organized as follows. Section II presents the scattering model. Section III computes the ergodic capacity. Section IV derives the trade-off between multiplexing and diversity gains. Section V illustrates the trade-off between multiplexing gain and propagation range. Finally, we will conclude this paper in Section VI.

In the following, we will use boldface capital letters for matrices and boldface small letter for vectors. For a vector $\mathbf{v}$, $\hat{\mathbf{v}}$ is a unit vector denoting its direction. $\mathbf{I}$ is the identity matrix. The determinant of a square matrix $\mathbf{A}$ is denoted by $\det(\mathbf{A})$ and its trace by $\mathrm{tr}(\mathbf{A})$. Two matrices related by $\mathbf{A} \succ \mathbf{B}$ implies that $\mathbf{A} - \mathbf{B}$ is positive definite. $\mathcal{C}^n$ and $\mathcal{C}^{n \times m}$ denote the set of $n$-dimensional complex vectors and $n \times m$ complex matrices respectively. $(\cdot)^*$, $(\cdot)^\dagger$ and $\mathsf{E}[\cdot]$ denote the conjugate, conjugate-transpose and expectation operations respectively. For an uncountable set $\mathcal{S}$, $|\mathcal{S}|$ denotes its Lebesgue measure. $\mathcal{CN}(\mu, \sigma^2)$ denotes a complex Gaussian random variable with mean $\mu$ and variance $\sigma^2$, and $\mathcal{CN}(\mathbf{M}, \mathbf{C} \otimes \mathbf{D})$ denotes a complex Gaussian random matrix with mean $\mathbf{M}$ and covariance $\mathbf{C} \otimes \mathbf{D}$ where $\otimes$ is the Kronecker product. Two random variables related by $x \sim y$ means that they are statistically the same. $\lceil x \rceil$ gives the smallest integer equal to or greater than $x$.

## II. SCATTERING MODEL

Following [11], we use the continuous-array model which eliminates the need to specify *a priori* the number of antennas and their relative positions. The commonly used MIMO model is a sampled version of it. Linear arrays are used to bring out the key concept. In a frequency non-selective fading channel, the transmit and the receive signals, $x(p)$ and $y(q)$, at a particular time are related by

$$y(q) = \int c(q,p) x(p) \, dp + z(q) \tag{2}$$

The channel response $c(p,q)$ gives the signal arrived at point $q$ on the receive array due to a unit point source applied at point $p$ on the transmit array. The additive noise $z(\cdot)$ is a white complex Gaussian random process with zero mean. The input signal is normalized such that $\mathsf{E}\big[\|x(p)\|^2\big] = \mathsf{SNR}$, the transmit SNR.

The channel response is a composition of array responses and scattering response:

$$c(q,p) = \iint a_r^*(\beta, q) h(\beta, \alpha) a_t(\alpha, p) \, d\alpha \, d\beta \tag{3}$$

In the expression, the *positions $p$ and $q$ are normalized to a wavelength* for conciseness. In the far-field, the array responses are given by

$$a_t(\alpha, p) = e^{-j2\pi\alpha p}, \quad |p| \le \frac{L_t}{2} \tag{4a}$$

$$a_r(\beta, q) = e^{-j2\pi\beta q}, \quad |q| \le \frac{L_r}{2} \tag{4b}$$

where $\alpha := \cos\theta$ is the directional cosine with respect to the axis of the transmit array and $\beta := \cos\vartheta$ is that with respect to the receive array (see Fig. 1). The length $L_t$ and $L_r$ denote the normalized length of the transmit and the receive arrays respectively. Note that we only consider the array responses, and ignore the mutual coupling between adjacent antenna elements and between the antenna element and its surroundings.
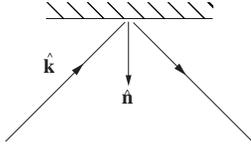
Fig. 3. Illustrates specular reflection.



Fig. 4. Illustrates diffuse scattering from a cluster of scatterers.

When antennas are putting closer to each other, there is mutual coupling among them that should not be ignored [16], [17]. In this case, the array response can be modeled as a product of the array response assuming no coupling and the active element response [18], [19]. The active element response then depends on the antenna spacing. To obtain a reasonable model for the active element response would require more information about the antenna type, and the dielectric properties of the antenna itself and its surroundings which is out of the scope of this paper.

The scattering response $h(\beta, \alpha)$ gives the signal received from direction $\beta$ due to a unit impulse radiated to direction $\alpha$. It captures the scattering condition of physical environment. As scattered paths are typically clustered around a number of disjoint angular intervals, $h(\cdot, \cdot)$ is non-zero in multiple sub-intervals only. With reference to Fig. 1, suppose there are $M_t$ scattering clusters illuminated by the transmit array with angular sub-intervals $\Theta_{t,i}$ ($i = 1, \cdots, M_t$) and $M_r$ clusters observed from the receive array with sub-intervals $\Theta_{r,i}$ ($i = 1, \cdots, M_r$). Defining $\Omega_{t,i} := \{\cos\theta : \theta \in \Theta_{t,i}\}$ and $\Omega_{r,j} := \{\cos\vartheta : \vartheta \in \Theta_{r,j}\}$, and denoting $\Omega_t := \bigcup_{i=1}^{M_t} \Omega_{t,i}$ and $\Omega_r := \bigcup_{i=1}^{M_r} \Omega_{r,i}$, the scattering response satisfies

$$h(\beta, \alpha) \neq 0 \quad \text{only if} \quad (\beta, \alpha) \in \Omega_r \times \Omega_t \qquad (5)$$

We will next model $h(\cdot, \cdot)$ within the non-zero region $\Omega_r \times \Omega_t$.

Three scattering mechanisms are considered. The choice of them is inspired by how they affect the path-loss exponent in the log-distance path-loss model, a classical propagation model used to estimate the received signal strength as a function of transmit-receive separation. The path-loss exponent due to specular reflection is around 2 whereas the exponent due to diffuse scattering depends on the number of bouncing encountered by physical paths before reaching the receiver. When it is single-bounce, the exponent is around 4. In the case of multi-bounce, the exponent is around $2(\nu + 1)$ where $\nu$ denotes the number of scattering clusters along the physical path. For example, the multi-bounce diffuse scattering shown in Fig. 2 has an exponent of around 6. The larger the exponent is, the more diffuse the channel is, and the less dependence in the joint response would be. Channel measurements [13] report that the path-loss exponent ranges from 2 up to 6 with typical values between 2 and 4. This implies that there is substantial dependence in the joint response. Analyses based on the Kronecker model are therefore not sufficient.

*Specular Reflection*

Starting with specular reflection, it occurs when the scattering source is smooth and large as compared to a wavelength, for examp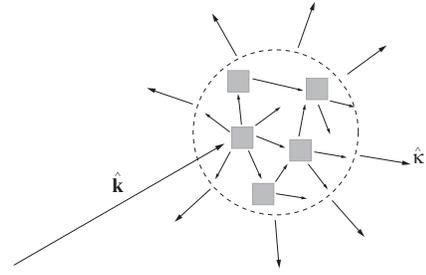le, back-wall reflection. The incident and reflected directions make equal angles from the surface normal. With reference to Fig. 3, suppose $\hat{\mathbf{n}}_i$ is the unit normal of the $i$th scattering cluster. For an impulse applied in the direction $\hat{\mathbf{k}} = [\sin\theta \ \cos\theta]^\dagger$, the signal received from the direction $\hat{\boldsymbol{\kappa}} = [\sin\vartheta \ \cos\vartheta]^\dagger$ is

$$e^{-j2\pi f_c \tau_i(\hat{\mathbf{k}})} \delta(\hat{\boldsymbol{\kappa}} - \boldsymbol{\Theta}(\hat{\mathbf{n}}_i)\hat{\mathbf{k}}) \, \boldsymbol{\Gamma}_{SP,i}(\hat{\mathbf{n}}_i \times \hat{\mathbf{k}}, \hat{\mathbf{k}}) \qquad (6)$$

for $\hat{\mathbf{k}} \in \Omega_{t,i}$, $i = 1, \cdots, M_t$, where $f_c$ is the carrier frequency, $\tau_i(\hat{\mathbf{k}})$ is the propagation delay along $\hat{\mathbf{k}}$, $\boldsymbol{\Theta}(\hat{\mathbf{n}}_i) = \mathbf{I} - 2\hat{\mathbf{n}}_i\hat{\mathbf{n}}_i^\dagger$ gives the rotation on the transmit direction, and $\boldsymbol{\Gamma}_{SP,i}(\cdot, \cdot)$ denotes the change in polarization[1]. The response is inherently *deterministic*, and the transmit and receive directions are in *one-to-one correspondence*. Furthermore, as $\|\boldsymbol{\Theta}(\hat{\mathbf{n}}_i)\|$ is unity implying $|d\hat{\boldsymbol{\kappa}}| = |d\hat{\mathbf{k}}|$, that is, $|\Omega_{t,i}| = |\Omega_{r,i}|$, we model the specular response as

$$h_{SP}(\beta, \alpha) = e^{-j2\pi f_c \tau(\alpha)} \delta(\beta - \alpha), \quad \beta, \alpha \in \Omega_t = \Omega_r \quad (7)$$

Note that only the measures $|\Omega_{t,i}|$ and $|\Omega_{r,i}|$ are required to be the same whereas the sets $\Omega_{t,i}$ and $\Omega_{r,i}$ need not be the same. For convenience, we assume that they are the same.

*Diffuse Scattering*

Diffuse scattering occurs when the scattering source is composed of a volume of small discrete scatterers, small as compared to a wavelength, for example, scattering by furniture. Upon impinging, the incident fields induce electric and magnetic dipoles on each discrete scatterer. The induced dipoles then *re-radiate* energy to directions other than the incident direction, like a *secondary source* or *passive relay*, as shown in Fig. 4. Let us look at the response of the $i$th scattering cluster. Suppose $\mathbf{r}_n$ is the position of the $n$-th scatterer relative to the centroid of the cluster. For an impulse applied to the direction $\hat{\mathbf{k}}$, the signal scattered to the direction $\hat{\boldsymbol{\kappa}}$ can be approximated by the Rayleigh scattering mechanism [20] and is

$$\frac{1}{\sqrt{N}} \sum_{n=1}^{N} e^{j\mathbf{k}_{e,i}^\dagger(\hat{\boldsymbol{\kappa}}, \hat{\mathbf{k}})\mathbf{r}_n} \boldsymbol{\Gamma}_{SD,i}(\hat{\boldsymbol{\kappa}}, \hat{\mathbf{k}}) \qquad (8)$$

---

[1]The polarization matrix for specular reflection is given by

$$\boldsymbol{\Gamma}_{SP,i}(\mathbf{v}, \hat{\mathbf{k}}) = \frac{\eta_2\sqrt{1-v^2} - \sqrt{\eta_1^2 - \eta_2^2 v^2}}{\eta_2\sqrt{1-v^2} + \sqrt{\eta_1^2 - \eta_2^2 v^2}} \, \hat{\mathbf{v}}\hat{\mathbf{v}}^\dagger$$
$$- \frac{\eta_1^2/\eta_2\sqrt{1-v^2} - \sqrt{\eta_1^2 - \eta_2^2 v^2}}{\eta_1^2/\eta_2\sqrt{1-v^2} + \sqrt{\eta_1^2 - \eta_2^2 v^2}} (\hat{\mathbf{v}} \times \hat{\mathbf{k}})(\hat{\mathbf{v}} \times \hat{\mathbf{k}})^\dagger$$

where $v$ is the magnitude of $\mathbf{v}$, and $\eta_1$ and $\eta_2$ are the intrinsic impedance of free space and the scattering cluster respectively.

where $\mathbf{k}_{e,i}(\hat{\boldsymbol{\kappa}}, \hat{\mathbf{k}})$ is the effective wavenumber vector of the scattering cluster along impinging direction $\hat{\mathbf{k}}$ and scattered direction $\hat{\boldsymbol{\kappa}}$, and $\boldsymbol{\Gamma}_{SD,i}(\cdot, \cdot)$ is the polarization matrix[2]. Compared to specular reflection, the response is inherently *stochastic*, and the transmit and receive directions are no longer in one-to-one correspondence. As the size of scattering cluster is typically large as compared to a wavelength and contains a lot of discrete scatterers, the displacement vector $\mathbf{r}_n$ can be modeled as a random variable in space and the phase lag $\mathbf{k}_{e,i}^{\dagger}(\hat{\boldsymbol{\kappa}}, \hat{\mathbf{k}})\mathbf{r}_n$ is approximately uniformly distributed in $[0, 2\pi)$. By the central limit theorem,

$$\frac{1}{\sqrt{N}} \sum_{n=1}^{N} e^{j\mathbf{k}_{e,i}^{\dagger}(\hat{\boldsymbol{\kappa}}, \hat{\mathbf{k}})\mathbf{r}_n} \sim \mathcal{CN}(0, 1)$$

and is a function of $\hat{\boldsymbol{\kappa}}$ and $\hat{\mathbf{k}}$. Ignoring polarization effect, the response of a single cluster is then a complex Gaussian random process with zero mean. The second order statistics depend on the density or roughness of the cluster as well as its dielectric properties. Without further information about the characteristics of the scattering cluster, we will model it as a white process over the angular intervals subtended by the cluster. Furthermore, we assume that clusters are uncorrelated. As a result, the single-bounce diffuse response $h_{SD}(\beta, \alpha)$ satisfies

$$\mathsf{E}\big[h_{SD}(\beta, \alpha) h_{SD}^*(\beta', \alpha')\big] = \delta(\beta - \beta')\delta(\alpha - \alpha'),$$
$$(\beta, \alpha) \in \bigcup_{i=1}^{M_t} \Omega_{r,i} \times \Omega_{t,i} \quad (9)$$

Because of the secondary-source property of diffuse scattering, the multi-bounce diffuse response is a convolution of single-bounce diffuse responses. The signal radiated to $\theta \in \Theta_{t,i}$ ($i = 1, \cdots, M_t$) is spreaded out and reaches the receiver from all directions over $\Theta_{r,1} \cup \cdots \cup \Theta_{r,M_r}$, as illustrated in Fig. 2b. Now, we can model the multi-bounce diffuse response as $\nu - 1$ convolution of independent complex Gaussian processes, each having the form of (9) where $\nu$ is the number of bouncing encountered by physical paths. But this would be difficult for closed-form analyses. To make the model more tractable while preserving the unique property of multi-bounce diffuse channel, we model the multi-bounce diffuse response, $h_{MD}(\beta, \alpha)$ as a zero-mean uncorrelated complex Gaussian random process satisfying

$$\mathsf{E}\big[h_{MD}(\beta, \alpha) h_{MD}^*(\beta', \alpha')\big] = \frac{1}{l^{\nu-1}}\delta(\beta - \beta')\delta(\alpha - \alpha'),$$
$$(\beta, \alpha) \in \Omega_r \times \Omega_t \quad (10)$$

where $l$ denotes the transmitter-receiver separation. The normalization by $l^{\nu-1}$ is due to the differential from the $\nu - 1$ convolution operations.

In general, the scattering response $h(\beta, \alpha)$ is a superposition of $h_{SP}(\beta, \alpha)$, $h_{SD}(\beta, \alpha)$, and $h_{MD}(\beta, \alpha)$. Those component

---

[2]The polarization matrix for diffuse scattering is given by

$$\boldsymbol{\Gamma}_{SD,i}(\hat{\boldsymbol{\kappa}}, \hat{\mathbf{k}}) = \frac{\epsilon_r - 1}{\epsilon_r + 2}\left(\mathbf{I} - \hat{\mathbf{k}}\hat{\mathbf{k}}^{\dagger}\right) + \frac{\mu_r - 1}{\mu_r + 2}\left(\hat{\boldsymbol{\kappa}}\hat{\mathbf{k}}^{\dagger} - \hat{\boldsymbol{\kappa}}^{\dagger}\hat{\mathbf{k}}\mathbf{I}\right)$$

where $\epsilon_r$ and $\mu_r$ are the relative permittivity and relative permeability of the scatterers respectively.

responses have very different path-loss exponent. Depending on the physical environment and the carrier frequency, $h(\beta, \alpha)$ is usually dominated by one of them. Therefore, we will perform analyses on them individually.

## III. CAPACITY

As the channel responses are continuous, we will apply singular function expansion and result from Landau and Widom [21] on the singular value distribution to compute the capacity for the specular, multi-bounce diffuse, and single-bounce diffuse channels.

### A. Specular Channel

In (3), the scattering response is sandwiched between two integral kernels:

$$a_t(\alpha, p), \quad (\alpha, p) \in \Omega_t \times [-L_t/2, L_t/2] \quad (11\text{a})$$
$$a_r(\beta, q), \quad (\beta, q) \in \Omega_r \times [-L_r/2, L_r/2] \quad (11\text{b})$$

As these kernels are non-zero and square integrable, there exist two sets of orthonormal functions $\{\eta_{t,m}(\alpha)\}$ and $\{\xi_{t,m}(p)\}$, and a sequence of positive numbers in a decreasing order $\{\sigma_{t,m}\}$ such that

$$a_t(\alpha, p), \quad (\alpha, p) \in \Omega_t \times [-L_t/2, L_t/2]$$
$$= \sum_{m=1}^{\infty} \sigma_{t,m}\eta_{t,m}(\alpha)\xi_{t,m}(p) \quad (12)$$

The expansion is equivalent to the singular value decomposition on finite dimensional matrices and $\sigma_{t,m}$'s are the singular values. Similarly,

$$a_r(\beta, q), \quad (\beta, q) \in \Omega_r \times [-L_r/2, L_r/2]$$
$$= \sum_{n=1}^{\infty} \sigma_{r,n}\eta_{r,n}(\beta)\xi_{r,n}(q) \quad (13)$$

We project the scattering response onto the set of singular functions $\{\eta_{r,n}^*(\beta)\eta_{t,m}(\alpha)\}$, the input signal onto $\{\xi_{t,m}(p)\}$, and the output signal and additive noise onto $\{\xi_{r,n}(q)\}$. The input-output model in (2) and (3) becomes

$$y_n = \sum_{m=1}^{\infty} \sigma_{r,n}H_{nm}\sigma_{t,m}x_m + z_n, \quad n = 1, 2, \cdots \quad (14)$$

For the specular channel,

$$H_{nm} = \int e^{-j2\pi f_c \tau(\alpha)}\eta_{r,n}^*(\alpha)\eta_{t,m}(\alpha)\, d\alpha \quad (15)$$

To keep up the deterministic nature of specular channel, we assume that

$$H_{nm} = e^{-j\phi_{nm}}\int \eta_{r,n}^*(\alpha)\eta_{t,m}(\alpha)\, d\alpha \quad (16)$$

The assumption is justified for large arrays due to their good angular resolution. When $L_t = L_r$,
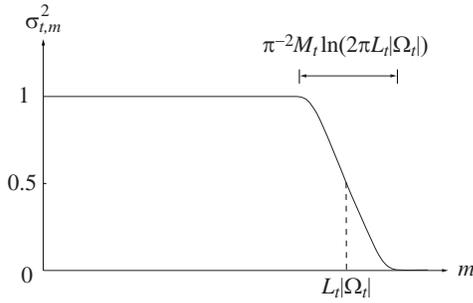
$$H_{nm} = e^{-j\phi_{nn}}\delta_{nm} \quad (17)$$

Fig. 5. Plots the distribution of $\sigma_{t,m}^2$ for large $L_t|\Omega_t|$.

which is diagonal. When $L_t \neq L_r$, we expect it as band diagonal. For simplicity, this paper focuses on $L_t = L_r$. The inputs and outputs in (14) are then related by

$$y_n = e^{-j\phi_{nn}}\sigma_{t,n}^2 x_n + z_n, \quad n = 1, 2, \cdots \quad (18)$$

The channel is composed of multiple parallel sub-channels. The capacity is therefore obtained by waterfilling over these sub-channels and is summarized in the following lemma.

*Lemma 3.1:* Suppose $\Omega_r$ and $\Omega_t$ are known a priori at the transmitter and the receiver respectively, $L_t = L_r$, and the receiver estimates $\phi_{nn}$'s. The capacity of specular channel is

$$C_{SP} = \left[ L_t|\Omega_t| + M_t \ln(2\pi L_t|\Omega_t|)f_1(\mathsf{SNR}) \right]$$
$$\log\left(1 + \frac{\mathsf{SNR}}{L_t|\Omega_t|}\right) + o\left(\ln(L_t|\Omega_t|)\right) \quad (19)$$

as $L_t|\Omega_t| \to \infty$, where

$$f_1(\mathsf{SNR}) = \frac{1}{4\pi^2}\ln\frac{\mathsf{SNR}}{L_t|\Omega_t|} + o(\ln\mathsf{SNR}) \quad (20)$$

as $\mathsf{SNR} \to \infty$.

To prove the above lemma, we need to know the distribution of $\sigma_{t,m}^2$. Fortunately, Landau and Widom [21] showed that the number of $\sigma_{t,m}^2$ greater than $x$ is given by

$$\bar{G}(x) = L_t|\Omega_t| + \frac{1}{\pi^2}M_t \ln(2\pi L_t|\Omega_t|)\ln\frac{1-x}{x} + o\left(\ln(L_t|\Omega_t|)\right) \quad (21)$$

as $L_t|\Omega_t| \to \infty$. This formula was first conjectured by Slepian in 1965 for the case when $M_t = 1$ [22]. It gave a precise interpretation of the $2WT$ degrees of freedom in a class of signals that are approximately time-limited to $[-T/2, T/2]$ and frequency-limited to $[-W, W]$ in [23]. Later in 1980, Landau and Widom proved the result for arbitrary $M_t$ [21].

To get an idea, Fig. 5 plots the distribution of $\sigma_{t,m}^2$. There are approximately $L_t|\Omega_t| - M_t \ln(2\pi L_t|\Omega_t|)/(2\pi^2)$ number of $\sigma_{t,m}^2$'s equal to 1, and $M_t \ln(2\pi L_t|\Omega_t|)/\pi^2$ in between 0 and 1. When $L_t|\Omega_t|$ is large, those in between 0 and 1 are negligible. But when $L_t|\Omega_t|$ is not large, the fraction of $\sigma_{t,m}^2$'s in the transition region becomes significant. Based on the Landau-Widom formula, we derive the asymptotic cumulative distribution of $\sigma_{t,m}^2$. The result is summarized in the following lemma.

*Lemma 3.2:* Define

$$G(x) := -\frac{1}{\pi^2}M_t \ln(2\pi L_t|\Omega_t|)\ln\frac{1-x}{x} \quad (22)$$

for $0 < x < \varepsilon$, where $\varepsilon$ satisfies

$$\ln\frac{\varepsilon}{1-\varepsilon} = -\frac{\pi^2 L_t|\Omega_t|}{M_t \ln(2\pi L_t|\Omega_t|)} \quad (23)$$

For any increasing and bounded function $f(x)$, we have

$$\sum_{x\in\{\sigma_{t,m}^2\},\, x\geq a} f(x) = \int_a^{1-\varepsilon} f(x)\, dG(x) + o\left(\ln(L_t|\Omega_t|)\right) \quad (24)$$

Now, the capacity of the specular channel can be written as

$$C_{SP} = \sum_{x\in\{\sigma_{t,m}^2\}} \log(x^2\mu)^+ \quad (25a)$$
$$= \int_{1/\sqrt{\mu}}^{1-\varepsilon} \left(\log(x^2\mu)\right)^+ dG(x) + o\left(\ln(L_t|\Omega_t|)\right) \quad (25b)$$

where $\mu$ satisfies

$$\mathsf{SNR} = \sum_{x\in\{\sigma_{t,m}^2\}} \left(\mu - \frac{1}{x^2}\right)^+ \quad (26a)$$
$$= \int \left(\mu - \frac{1}{x^2}\right)^+ dG(x) + o\left(\ln(L_t|\Omega_t|)\right) \quad (26b)$$

The rest of the proof for Lemma 3.1 is included in Appendix I.

### B. Diffuse Channels

We start with the multi-bounce diffuse channel where we have

$$H_{nm} = \iint \eta_{r,1}^*(\beta)h_{MD}(\beta,\alpha)\eta_{t,1}(\alpha)\, d\alpha d\beta \quad (27a)$$
$$\overset{(a)}{\sim} \frac{1}{l^{(\nu-1)/2}} \int_{\Omega_r} \int_{\Omega_t} \eta_{r,1}^*(\beta)h_w(\beta,\alpha)\eta_{t,1}(\alpha)\, d\alpha d\beta \quad (27b)$$
$$\overset{(b)}{\sim} \frac{1}{l^{(\nu-1)/2}} \iint \eta_{r,1}^*(\beta)h_w(\beta,\alpha)\eta_{t,1}(\alpha)\, d\alpha d\beta \quad (27c)$$
$$\overset{(c)}{\sim} \frac{1}{l^{(\nu-1)/2}} \mathcal{CN}(0,1) \quad (27d)$$

The $h_w(\beta,\alpha)$ is a white complex normal process over all $\beta$ and $\alpha$. As $h_{MD}(\beta,\alpha)$ is a zero-mean white complex Gaussian random process over $\Omega_r \times \Omega_t$, (a) holds. The singular functions $\eta_{r,n}(\cdot)$ and $\eta_{t,m}(\cdot)$ are non-zero only over $\Omega_r$ and $\Omega_t$ respectively so (b) holds. The circularly symmetric property of $h_w(\beta,\alpha)$ implies (c). In conjunction with the orthonormal property of the singular functions, $H_{nm}$'s are independent. Apparently, the channel now becomes the standard Kronecker MIMO model. However unlike the Kronecker model, the dimension of the fading matrix in our case is not known *a priori*. It depends on the scattering condition, array sizes, and the SNR. To compute the channel capacity, we will first derive a lower bound using tools from random matrix theory and then derive an upper bound. We will show that these bounds are asymptotically tight.

Note that the asymptotic cumulative distribution of $\sigma_{t,m}^2$ depends on $L_t|\Omega_t|$ and $M_t$ only. That is, two channels with different $\Omega_t$ but same measure $|\Omega_t|$ and same number of disjoint sub-intervals $M_t$ will yield the same performance for large $L_t$. For simplicity, this paper focuses on the scenario

where $L_t|\Omega_t| = L_r|\Omega_r|$ and $M_t = M_r$. That is, we consider the case where the asymptotic cumulative distribution of $\sigma_{t,m}^2$ and that of $\sigma_{r,n}^2$ are approximately the same.

For any $\epsilon$, if we consider only those $\sigma_{t,m}^2$'s greater than $\epsilon$ and pour equal power over them, this will give a lower bound. Recall that $\bar{G}(\epsilon)$ in (21) gives the number of $\sigma_{t,m}^2$ greater than $\epsilon$. We define the empirical distribution of $\sigma_{t,m}^2$ by

$$F_\epsilon(x) := \frac{\bar{G}(\epsilon) - \bar{G}(x)}{\bar{G}(\epsilon)} \tag{28}$$

and its inverse map by $F_\epsilon^{-1}(x)$. For a fixed $\epsilon$, as $L_t|\Omega_t|$ increases, random matrix results in Girko [24] are applied to obtain the limiting eigenvalue distribution for $l^{1-\nu}\mathbf{\Sigma}_\epsilon^2\mathbf{H}_\epsilon\mathbf{\Sigma}_\epsilon^2\mathbf{H}_\epsilon^\dagger$, denoted by $F_c(x)$, where $\mathbf{\Sigma}_\epsilon$ is a diagonal matrix of dimension $\bar{G}(\epsilon)$ with the $n$th diagonal element being $\sigma_{t,n}$ and $\mathbf{H}_\epsilon$ is a $\bar{G}(\epsilon) \times \bar{G}(\epsilon)$ matrix with the $(n,m)$th element being $H_{nm}$. [3] showed that the Steltjes' transform[3] of $F_c(x)$ is given by

$$m_{F_c}(z) = \int_0^1 u(x,z)\,dx$$

and $u(x,z)$ is the unique solution to the fixed-point equation

$$u(x,z)$$
$$= \left[-z + F_\epsilon^{-1}(x)\int_0^1 \frac{F_\epsilon^{-1}(p)\,dp}{1 + F_\epsilon^{-1}(p)\int_0^1 u(q,z)F_\epsilon^{-1}(q)\,dq}\right]^{-1}$$

Hence, the capacity of multi-bounce diffuse channel, $C_{MD}$ is lower-bounded by

$$C_{MD} \geq \bar{G}(\epsilon)\int_0^\infty \log\left(1 + \frac{\mathsf{SNR}}{l^{\nu-1}}x\right)dF_c(x) \tag{29}$$

At high SNR, it approximates

$$C_{MD} \gtrsim \bar{G}(\epsilon)\left[\log\frac{\mathsf{SNR}}{l^{\nu-1}e} + 2\int_0^1 \log F_\epsilon^{-1}(x)\,dx\right] \tag{30a}$$

$$= \bar{G}(\epsilon)\left[\log\frac{\mathsf{SNR}}{l^{\nu-1}e} + 2\int_\epsilon^1 \log x\,dF_\epsilon(x)\right] \tag{30b}$$

The lower-bound is computed and summarized in the following lemma, and the proof is included in Appendix II.

*Lemma 3.3:* Suppose $\Omega_r$ and $\Omega_t$ are known a priori at the transmitter and the receiver respectively, $L_t|\Omega_t| = L_r|\Omega_r|$, $M_t = M_r$, and $H_{nm}$'s are known at the receiver. The ergodic capacity of the multi-bounce diffuse channel is approximately lower-bounded by

$$C_{MD} \gtrsim \left[L_t|\Omega_t| + M_t\ln(2\pi L_t|\Omega_t|)f_2(\mathsf{SNR})\right]\log\frac{\mathsf{SNR}}{l^{\nu-1}e}$$
$$+ o\big(\ln(L_t|\Omega_t|)\big) \tag{31}$$

as $L_t|\Omega_t| \to \infty$, where

$$f_2(\mathsf{SNR}) = \frac{1}{4\pi^2}\ln\frac{\mathsf{SNR}}{l^{\nu-1}} + o(\ln\mathsf{SNR}) \tag{32}$$

as $\mathsf{SNR} \to \infty$.

[3]The Steltjes' transform of a distribution $F(\cdot)$ is defined by

$$m_F(z) := \int \frac{1}{x-z}\,dF(x)$$

Because $\sigma_{t,m}^2$'s are less than 1 and $\log\det$ is concave, the capacity is therefore upper-bounded by

$$C_{MD} \leq \sum_m \log\left(1 + \frac{\mathsf{SNR}}{l^{\nu-1}}\sigma_{t,m}^2\right) \tag{33a}$$

$$= \int_0^{1-\varepsilon} \log\left(1 + \frac{\mathsf{SNR}}{l^{\nu-1}}x\right)dG(x) + o\big(\ln(L_t|\Omega_t|)\big) \tag{33b}$$

It is computed in Appendix III and the result is summarized by the following lemma.

*Lemma 3.4:* Suppose $\Omega_r$ and $\Omega_t$ are known a priori at the transmitter and the receiver respectively, $L_t|\Omega_t| = L_r|\Omega_r|$, $M_t = M_r$, and $H_{nm}$'s are known at the receiver. The ergodic capacity of the multi-bounce diffuse channel is upper-bounded by

$$C_{MD} \leq \left[L_t|\Omega_t| + M_t\ln(2\pi L_t|\Omega_t|)f_3(\mathsf{SNR})\right]\log\left(1 + \frac{\mathsf{SNR}}{l^{\nu-1}}\right)$$
$$+ o\big(\ln(L_t|\Omega_t|)\big) \tag{34}$$

as $L_t|\Omega_t| \to \infty$, where

$$f_3(\mathsf{SNR}) = \frac{1}{2\pi^2}\ln\frac{\mathsf{SNR}}{l^{\nu-1}} + o(\ln\mathsf{SNR}) \tag{35}$$

as $\mathsf{SNR} \to \infty$.

Now, we proceed to the single-bounce diffuse channel. When $L_t$ and $L_r$ are large, the single-bounce channel is approximately equivalent to $M_t$ independent single-cluster multi-bounce diffuse channels. Fischer's inequality assures that the optimal input covariance is separable among the $M_t$ parallel clustered channels. Asymptotic results from multi-bounce diffuse channel are applied to obtain the asymptotic capacity of single-bounce diffuse channel and is summarized in Theorem 3.5.

### C. Asymptotic Maximum Multiplexing Gain

*Theorem 3.5:* Suppose $\Omega_t$ and $\Omega_r$ are known a priori at the transmitter and the receiver respectively.

- Specular channels. Assume $L_t = L_r$. The channel capacity is

$$C_{SP} = L_t|\Omega_t|\log\left(1 + \frac{\mathsf{SNR}}{L_t|\Omega_t|}\right) + o(L_t|\Omega_t|) \tag{36}$$

as $L_t|\Omega_t| \to \infty$.

- Multi-bounce diffuse channels. Assume $L_t|\Omega_t| = L_r|\Omega_r|$ and $M_t = M_r$. The ergodic capacity is bounded by

$$L_t|\Omega_t|\log\frac{\mathsf{SNR}}{l^{\nu-1}e} + o(L_t|\Omega_t|)$$
$$\lesssim C_{MD} \leq L_t|\Omega_t|\log\left(1 + \frac{\mathsf{SNR}}{l^{\nu-1}}\right) + o(L_t|\Omega_t|) \tag{37}$$

as $L_t|\Omega_t| \to \infty$.

- Single-bounce diffuse channels. Assume $L_t|\Omega_{t,i}| = L_r|\Omega_{r,j}| = \frac{L_t|\Omega_t|}{M_t}$ $\forall i, j$, and $M_t$ is finite. The ergodic capacity is bounded by

$$L_t|\Omega_t|\log\frac{\mathsf{SNR}}{M_t e} + o(L_t|\Omega_t|)$$
$$\lesssim C_{SD} \leq L_t|\Omega_t|\log\left(1 + \frac{\mathsf{SNR}}{M_t}\right) + o(L_t|\Omega_t|) \tag{38}$$

as $L_t|\Omega_t| \to \infty$.

Theorem 3.5 summaries the asymptotic capacity results. All channels have the same asymptotic number of spatial degrees of freedom equal to $L_t|\Omega_t|$ – the maximum spatial multiplexing gain. It is insensitive to the underlying scattering mechanisms. This result agrees with the degree-of-freedom formula in [11] where scattering mechanisms are not modeled. It supplements [11] with the capacity analysis for linear arrays. For other array geometries, the difficulty lies in finding the distribution for the singular values $\sigma_{t,m}$ and $\sigma_{r,n}$ which could be a possible extension of this work.

The underlying scattering mechanisms affect the received SNR on each spatially multiplexed channel. Several observations are worth pointing out:

- In the specular channel, as the transmit and the receive directions are in one-to-one correspondence, the received SNR per spatial channel is scaled by the number of spatial channels supported.
- In the multi-bounce diffuse channel, as the transmit power to a particular direction is spread out over the entire $\Omega_r$, there is no scaling of SNR by the number of spatial channels. This phenomenon is similar to the spreading gain in waveform channels where a data symbol can be spread over multiple time-samples and/or sub-carriers to increase the robustness against channel fading. In waveform channels, the spreading is done *explicitly* whereas in multiple-antenna channels, the secondary-source property of diffuse scattering brings forth the spreading *implicitly*. Also because of the secondary-source property of diffuse scattering, a fraction of power is lost in each bouncing and therefore the received SNR is scaled by $l^{(\nu-1)}$.
- In the single-bounce diffuse channel, the transmit power emanated from $\Omega_{t,i}$ is spread over $\Omega_{r,i}$ only so the receive SNR per spatial channel is scaled by the number of clusters only.

Finally, we reiterate that the spreading benefit and path loss counteract each other in diffuse channels. Similar observation is reported in [27]. In [7], [14], channel capacities are, however, shown to be increasing with less dependence between the transmit and the receive directions, that is, multi-bounce diffuse channels would have better performance than specular channels. The inconsistency stems from [7], [14] keeping the receive SNR per spatial channel constant while we are keeping the total SNR constant.

### D. SNR-Dependence of Usable Degrees of Freedom

At high SNR, the capacity of specular channel given in Lemma 3.1 can be approximated by

$$C_{SP} \approx \left[ L_t|\Omega_t| + \frac{1}{4\pi^2} M_t \ln(2\pi L_t|\Omega_t|) \ln \frac{\text{SNR}}{L_t|\Omega_t|} \right] \log \frac{\text{SNR}}{L_t|\Omega_t|} \tag{39}$$

while the capacity of multi-bounce diffuse channel given in Lemma 3.3–3.4 is approximately equal to

$$C_{MD} \approx \left[ L_t|\Omega_t| + \frac{1}{c\pi^2} M_t \ln(2\pi L_t|\Omega_t|) \ln \frac{\text{SNR}}{l^{\nu-1}} \right] \log \frac{\text{SNR}}{l^{\nu-1}} \tag{40}$$
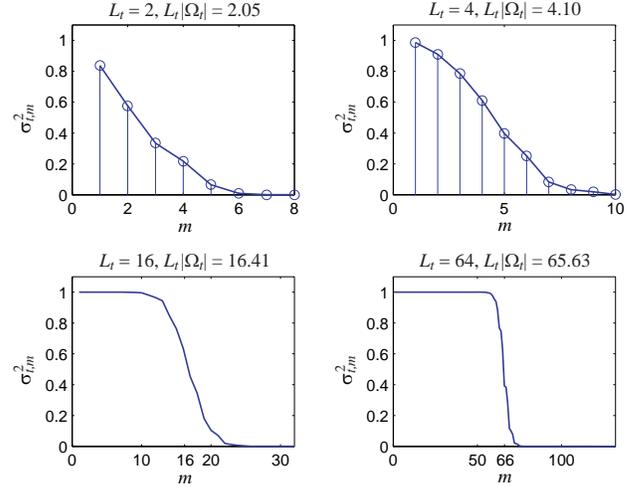


Fig. 6. Plots $\sigma_{t,m}^2$ for $\Theta_t = [25°, 55°] \cup [80°, 110°] \cup [145°, 175°]$ ($|\Omega_t| = 1.0254$) and $L_t$ varying from 2 to 64.

for some constant $c \in [2, 4]$. Apparently, there is an addition of $\frac{1}{4\pi^2} M_t \ln(2\pi L_t|\Omega_t|) \ln \frac{\text{SNR}}{L_t|\Omega_t|}$ degrees of freedom in the specular channel and $\frac{1}{c\pi^2} M_t \ln(2\pi L_t|\Omega_t|) \ln \frac{\text{SNR}}{l^{\nu-1}}$ in the multi-bounce diffuse channel. These additional degrees of freedom as compared to $L_t|\Omega_t|$ is negligible as $L_t|\Omega_t| \to \infty$ but become increasingly significant as $L_t|\Omega_t|$ reduces to more practical value.

The integral kernels in (11) have infinite number of non-zero singular values. In theory, if there is no noise, there will be an infinite number of degrees of freedom for information transmission. Because no matter how small the gain of a degree-of-freedom is, an infinite-precision system should be able to recover the signal carried by it. In practice, we cannot recover the signal carried by a degree-of-freedom that has gain far below the noise level. When $L_t$ and $L_r$ are large, the transition between good and bad singular values is so abrupt that the usable degrees of freedom is $L_t|\Omega_t|$. However when $L_t$ and $L_r$ are far from infinite, the distribution of singular values is smoother. To get an idea, Fig. 6 plots the distribution for different array sizes. In contrast to the discrete array model where the maximum spatial multiplexing gain does not depend on the SNR, the number of usable degrees of freedom in the continuous model depends on the noise level. That is, if we have the flexibility to place any number of antennas on the finite array aperture, it becomes difficult to define the maximum spatial multiplexing gain. If the aperture size does not go to infinity while the SNR does, the maximum spatial multiplexing gain would be infinite. The same argument can be obtained from the concept of super-resolution [28], [29].

How can the spatial multiplexing gain go to infinity for a finite aperture? In principle, any radiating system can generate infinite number of transmission modes implying that a small array can generate the same set of transmission modes as a large array. However, in order to excite transmission modes with the same strength on both arrays, one needs to pack at least the same amount of moving charges in both arrays. More power is needed to keep the charges in the small array than
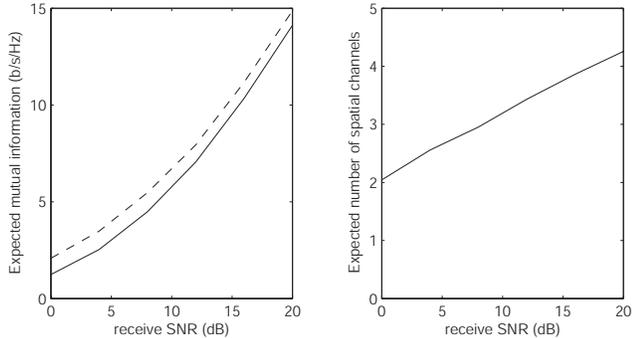
Fig. 7. Plots the expected mutual information versus the number of spatial channels at different receive SNR for $L_t = 2$. The dotted line shows the upper bound.

in the large array[4]. Therefore, a higher SNR is required for a smaller array to have the same number of usable degrees of freedom as a larger array. When SNR goes to infinity, the number of usable degrees of freedom goes to infinity as well.

The SNR-dependence implies that the number of antennas used should also depend on the SNR. To illustrate this point, let us look at a numerical example. We consider a multi-bounce diffuse channel with 3 randomly placed scattering clusters each of angle $30°$ ($\mathsf{E}\big[|\Omega_t|\big] = \mathsf{E}\big[|\Omega_r|\big] = 1$) and array length of 2 wavelength. Waterfilling is performed over singular values $\sigma_{t,m}^2$ to determine the number of spatial channels used and the amount of transmit power poured over them. The expected mutual information and the corresponding number of spatial channels for different receive SNR are plotted in Fig. 7. The upper bound shown is the ergodic capacity with full channel state information at both transmitter and receiver. The graph illustrates that the expected mutual information closely tracks the upper bound and the number of spatial channels increases with SNR. At receive SNR of 0 dB, the number of spatial channels is greater than $L_t|\Omega_t|$ on average. At receive SNR of 20 dB, the number of spatial channels is greater than $2L_t$ which corresponds to antenna spacing of less than half-wavelength.

## IV. DIVERSITY

Last section shows that the asymptotic ergodic capacity is insensitive to the underlying scattering mechanisms. In this section, we will show that these mechanisms have significant impact in slow fading channels. In particular, we will illustrate how the trading between spatial multiplexing gain and diversity gain varies with the underlying scattering mechanisms. The discussion in this section will focus on the large-array regime.

Asymptotically, there are $L_t|\Omega_t|$ significant $\sigma_{t,m}^2$ and $L_r|\Omega_r|$ significant $\sigma_{r,n}^2$, and these eigenvalues are all asymptotically equal to 1. The multi-bounce diffuse channel is therefore

[4]Since the amount of moving charges is the same, the small array has a higher current density than the large array. A higher current density, in turn, builds up a larger radiation reaction, the self force to hold charges together. Hence, the small array will have a poorer radiation efficiency because most of its energy is consumed to hold the charges in a small volume instead of radiating out.

approximately mimic the standard i.i.d. fading model for multiple-antenna systems where the maximum diversity gain is $L_t L_r|\Omega_t||\Omega_r|$. Similarly, the single-bounce diffuse channel is approximately modeled by

$$
\mathbf{y} = \begin{bmatrix} \mathbf{H}_1 & & \mathbf{0} \\ & \ddots & \\ \mathbf{0} & & \mathbf{H}_{M_t} \end{bmatrix} \mathbf{x} + \mathbf{z} \tag{41}
$$

where $\mathbf{H}_i \sim \mathcal{CN}\big(\mathbf{0}, \mathbf{I}_{L_r|\Omega_{r,i}|} \otimes \mathbf{I}_{L_t|\Omega_{t,i}|}\big)$ for $i = 1, \cdots, M_t$. The maximum diversity gain is $\sum_i L_t L_r|\Omega_{t,i}||\Omega_{r,i}|$.

Underlying scattering mechanisms not only affect the maximum diversity gain but also the trade-off between multiplexing gain and diversity gain. To illustrate this point, we use the trade-off formulation proposed in [15]. At a fixed target data rate, the outage probability would decay like $\mathsf{SNR}^{-d_0}$ at high SNR where $d_0$ is the maximum diversity gain. Increasing the target rate $R = r \log \mathsf{SNR}$ (bits/s/Hz), we would expect an increase in the outage probability or equivalently, the outage probability delays like $\mathsf{SNR}^{-d(r)}$ in which the exponent $d(r)$ is less than $d_0$ and decreases with increasing $r$. The curve $d(r)$ then characterizes the trade-off between the data rate (multiplexing gain) and diversity gain. A formal definition is given below. More in-depth discussions on its operational interpretation can be found in [30, Chapter 9]. Finally, other formulations such as using the variance of mutual information [31] can also be used to illustrate such a trade-off.

*Definition 4.1:* A diversity gain $d(r)$ is achieved at multiplexing gain $r$ if the data rate is

$$
R = r \log \mathsf{SNR},
$$

and the outage probability is

$$
P_{out}(R) \approx \mathsf{SNR}^{-d(r)}
$$

or more precisely,

$$
\lim_{\mathsf{SNR} \to \infty} \frac{\log P_{out}(r \log \mathsf{SNR})}{\log \mathsf{SNR}} = -d(r)
$$

The curve $d(r)$ characterizes the multiplexing-diversity trade-off of the channel.

As the multi-bounce diffuse channel mimic the standard i.i.d. fading channel, the trade-off curve $d_{MD}(r)$ has solved in [15]. For the single-bounce diffuse channel, the trade-off curve $d_{SD}(r)$ is given by solving

$$
\lim_{\mathsf{SNR} \to \infty} \frac{\log P\big[\prod_{i=1}^{M_t} \det(\mathbf{I} + \mathsf{SNR}\mathbf{H}_i^\dagger \mathbf{H}_i) < \mathsf{SNR}^r\big]}{\log \mathsf{SNR}}
$$
$$
= -d_{SD}(r) \tag{42}
$$

The curve is computed in Appendix IV and is summarized in Theorem 4.2.

*Theorem 4.2:* Suppose $\Omega_t$ and $\Omega_r$ are known a priori at the transmitter and the receiver respectively, and $H_{nm}$'s are known at the receiver. Denote the maximum multiplexing gain as
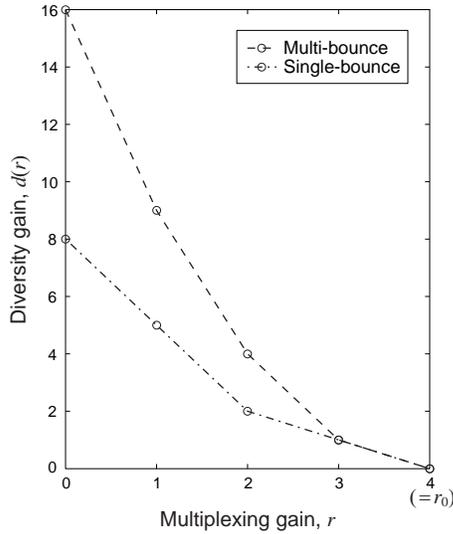
$$
r_0 := \min\big\{L_t|\Omega_t|, L_r|\Omega_r|\big\}
$$

Fig. 8. Contrasts the multiplexing-diversity trade-off curves for the multi-bounce and the single-bounce diffuse channels where $M_t = M_r = 2$, $L_t|\Omega_{t,i}| = 2$, and $L_r|\Omega_{r,i}| = 2$ for $i = 1, 2$.



Fig. 9. A physical environment with an infinite line of scattering clusters in the midway between transmitter and receiver.

- Multi-bounce diffuse channels. The trade-off curve is given by a piecewise linear function connecting the points $(r, d_{MD}(r))$, $r = 0, \cdots, r_0$, where

$$d_{MD}(r) = (L_t|\Omega_t| - r)(L_r|\Omega_r| - r) \qquad (43)$$

- Single-bounce diffuse channels. The trade-off curve is

$$d_{SD}(r) = d_1(r) \oplus d_2(r) \oplus \cdots \oplus d_{M_t}(r) \qquad (44)$$

where $d_i(r)$ is a piecewise linear function connecting the points $(r, d_i(r))$, $r = 0, \cdots, \min\{L_t|\Omega_{t,i}|, L_r|\Omega_{r,i}|\}$ and

$$d_i(r) = (L_t|\Omega_{t,i}| - r)(L_r|\Omega_{r,i}| - r) \qquad (45)$$

The operation $\oplus$ denotes the min-plus convolution and is defined as

$$(f \oplus g)(t) = \inf_{0 \le s \le t}\big\{f(t - s) + g(s)\big\} \qquad (46)$$

Descriptively, the trade-off curve is obtained by putting end-to-end the different linear pieces in $d_i(r)$'s, sorted by increasing slopes (or equivalently, decreasing negative slopes).

To get an idea on the differences in the trade-off, let us consider the scenario where the number of disjoint sub-intervals in $\Omega_t$ and $\Omega_r$ are equal, and the respective sub-intervals are of equal length. Then, $d_{SD}(r)$ is the piecewise linear function connecting the points $(m, d_{SD}(r))$, $r = 0, M_t, \cdots, r_0$, where

$$d_{SD}(r) = \frac{1}{M_t}(L_t|\Omega_t| - r)(L_r|\Omega_r| - r) \qquad (47)$$

Compared to $d_{MD}(r)$ in (43), the multi-bounce channel achieves an $M_t$-fold better diversity gain than the single-bounce channel in supporting a multiplexing gain which is a multiple of $M_t$. Fig. 8 plots the two curves for $r_0 = 4$ and $M_t = 2$.

Recent space-time code design mainly focuses on the i.i.d fading channel (equivalent to the multi-bounce diffuse channel). However, real channels are more specular and single-bounce diffuse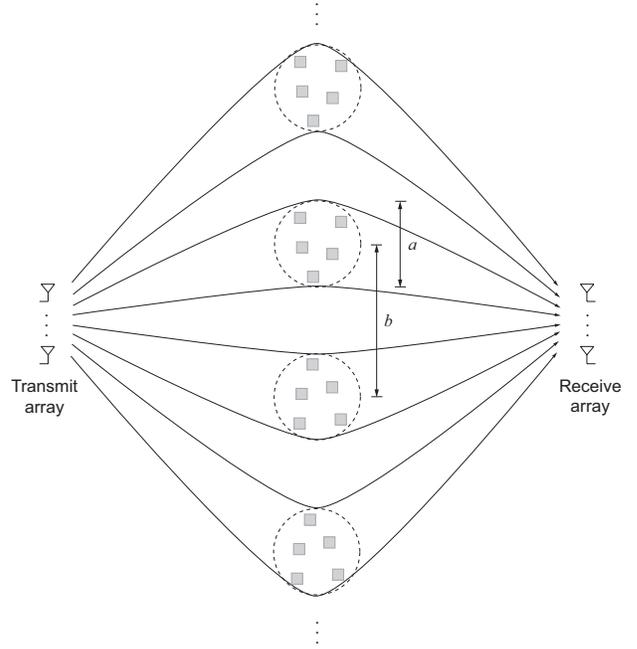 in nature. Understanding the differences on the trade-off sheds light on designing more efficient space-time coding schemes that can adapt to the physical environment. Imagining if we design a space-time code that is optimal for the i.i.d fading channel and use it in a single-bounce diffuse channel, the link reliability can be much worse.

Finally, it is possible to turn a single-bounce diffuse channel into a multi-bounce diffuse channel by increasing the antenna spacing. This plausibly increases the diversity gain and validate the performance analyses based on the i.i.d. fading model. However, when the array length is fixed, using less antennas decreases the spatial degrees of freedom. The resulting trade-off curve remains upper-bounded by the curve given in Theorem 4.2.

## V. PROPAGATION RANGE

As the scattering mechanisms are tied up with the path-loss model, the propagation range are therefore related to the multiplexing gain and diversity gain. For example, [27] points out the trade-off between path-loss and multiplexing gain across different scattering mechanisms: specular reflection has better path-loss but worse multiplexing gain whereas diffuse scattering has worse path-loss but better multiplexing gain. Under the *same* scattering mechanism, we will illustrate that there is also a trade-off between propagation range and multiplexing gain. The analysis involved is not as vigorous as that in previous sections on ergodic capacity and diversity gain. At the least, it gives us a more comprehensive perspective on the range-multiplexing-diversity trade-off.

If the scattering clusters remain fixed while the transmitter-receiver separation is changing, we would expect

$$|\Omega_t|, |\Omega_r| \propto \frac{1}{l} \qquad (48)$$

Recall that $l$ is the propagation range. As the asymptotic multiplexing gain is proportional to $|\Omega_t|, |\Omega_r|$, there exists a trade-off between multiplexing gain and propagation range under the same scattering mechanism. However, in general changing the transmitter-receiver separation will bring in or fade out scattering clusters. For example, Fig. 9 shows a physical environment where scattering clusters are located in the midway between transmitter and receiver. When the transmitter and receiver are farther apart, there are apparently more clusters visible by them. On the other hand, when they are closer, there are less clusters. Now let us compute the total angle spread. Denote the diameter of the cluster by $a$ and the cluster-cluster separation by $b$. The distance between the center of the $n$th cluster to the center of the antenna array is

$$\rho = \sqrt{(n+1/2)^2 b^2 + (l/2)^2}$$

The angle spread due to the $n$th cluster is

$$\frac{l/2}{\rho} \cdot \frac{a}{\rho} = \frac{la}{2\rho^2}$$

The total angle spread is therefore given by the sum

$$|\Omega_t| = |\Omega_r| = \frac{4a}{l} \sum_{n=0}^{\infty} \frac{1}{1 + (2n+1)^2 (b/l)^2} \quad (49)$$

If $b > a$, it is bounded by

$$\frac{\pi a}{bl}\left(1 - \frac{2}{\pi}\tan^{-1}\frac{b}{l}\right) \le |\Omega_t| = |\Omega_r| \le \frac{\pi a}{bl}\left(1 + \frac{2}{\pi}\tan^{-1}\frac{b}{l}\right) \tag{50}$$

implying

$$|\Omega_t| = |\Omega_r| = \frac{\pi a}{b}\frac{1}{l} + o(1/l) \tag{51}$$

for large $l$. The total angle spread remains inversely proportional to the propagation range. Suppose $|\Omega_{t0}|$ and $|\Omega_{r0}|$ are the respective transmit and receive angle spread at the reference range $l_0 = 1$m. We draw the following hypothesis:

$$|\Omega_t| = \frac{|\Omega_{t0}|}{l} \quad \text{and} \quad |\Omega_r| = \frac{|\Omega_{r0}|}{l} \tag{52}$$

Now to achieve a propagation range of $l$, the maximum multiplexing gain would be

$$r_0(l) = \frac{1}{l}\min\{L_t|\Omega_{t0}|, L_r|\Omega_{r0}|\}$$

One can sacrifice some of the multiplexing gain to obtain a better diversity gain. The trade-off involved depends on the underlying scattering mechanisms. Fig. 10 gives an example of such trade-offs among multiplexing gain, diversity gain, and propagation range for the case $r(l_0) = 4$ and $M_t = 2$.

## VI. CONCLUSIONS

We use the angular intervals subtended by clusters of scatterers to characterize the scattering condition, and study linear arrays that are limited in length but not the number of antennas. Then we model the response within those angular intervals due to basic scattering mechanisms. In the capacity analysis, we show that for arrays of length $L$ in a physical environment of total angle spread $|\Omega|$, the ergodic capacity increases linearly with $L|\Omega|$ for large arrays. But when antenna
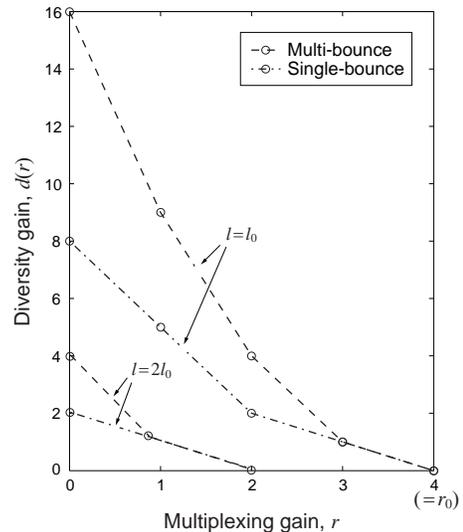


Fig. 10. Illustrates the multiplexing-diversity-range trade-offs for $M_t = M_r = 2$ at $l = l_0$ and $2l_0$.

arrays reduce to more practical sizes, the number of spatial degrees of freedom depends on the SNR as well. This implies that the number of antennas used would depend on the SNR. In the diversity analysis, we focus on the trade-off between multiplexing gain (data rate) and diversity gain. Unlike the ergodic capacity, the different scattering mechanisms have distinguishable trade-offs. These differences would give us more insights into space-time code design. Finally, we attempt to quantify the trade-off among propagation range, diversity gain, and multiplexing gain which gives us a more comprehensive perspective on the interplay between possible benefits of multiple-antenna systems.

## APPENDIX I
### PROOF OF LEMMA 3.1

First, we solve for $\mu$ in (26):

$$\mathsf{SNR} = \int \left(\mu - \frac{1}{x^2}\right)^+ dG(x) + o\big(\ln(L_t|\Omega_t|)\big)$$

$$= (\mu-1)L_t|\Omega_t| + \frac{1}{\pi^2}M_t\ln(2\pi L_t|\Omega_t|)\Big[(\mu-1)$$

$$\ln(\sqrt{\mu}-1) - \frac{\mu}{2} - \sqrt{\mu} + \frac{1}{2(1-\varepsilon)^2} + \frac{1}{1-\varepsilon}\Big]$$

$$+ o\big(\ln(L_t|\Omega_t|)\big)$$

$$= (\mu-1)L_t|\Omega_t| + o\big(\ln(L_t|\Omega_t|)\big)$$

which gives

$$\mu = 1 + \frac{\mathsf{SNR}}{L_t|\Omega_t|} + o(1)$$

as $L_t|\Omega_t| \to \infty$. The capacity can be written as

$$C_{SP} = \int_{1/\sqrt{\mu}}^{1-\varepsilon} \log(x^2\mu)\, dG(x) + o\big(\ln(L_t|\Omega_t|)\big)$$

$$= \log\mu \int_{1/\sqrt{\mu}}^{1-\varepsilon} dG(x) + 2\int_{1/\sqrt{\mu}}^{1-\varepsilon} \log x\, dG(x)$$

$$+ o\big(\ln(L_t|\Omega_t|)\big)$$

The first integral is

$$L_t|\Omega_t| + \frac{1}{\pi^2} M_t \ln(2\pi L_t|\Omega_t|) \ln(\sqrt{\mu} - 1)$$

and the second integral is

$$\frac{1}{\pi^2 \ln 2} M_t \ln(2\pi L_t|\Omega_t|) \int_{1/\sqrt{\mu}}^{1-\varepsilon} \frac{\ln x}{x} + \frac{\ln x}{1-x} \, dx$$
$$= \frac{1}{\pi^2 \ln 2} M_t \ln(2\pi L_t|\Omega_t|) \Big[ \frac{1}{2} \ln^2(1-\varepsilon) - \frac{1}{8} \ln^2 \mu + \mathrm{Li}_2(\varepsilon)$$
$$- \mathrm{Li}_2(1 - 1/\sqrt{\mu}) \Big]$$

As $\varepsilon$ tends to 0 when $L_t|\Omega_t|$ tends to $\infty$, the capacity can be re-written as

$$C_{SP} = \Big[ L_t|\Omega_t| + M_t \ln(2\pi L_t|\Omega_t|) f_1(\mathsf{SNR}) \Big] \log \mu$$
$$+ o\big( \ln(L_t|\Omega_t|) \big)$$

as $L_t|\Omega_t| \to \infty$, where

$$f_1(\mathsf{SNR})$$
$$= \frac{1}{\pi^2} \Big[ \ln(\sqrt{\mu} - 1) - \frac{1}{4} \ln \mu - \frac{2}{\ln 2} \mathrm{Li}_2(1 - 1/\sqrt{\mu}) / \log \mu \Big]$$
$$= \frac{1}{4\pi^2} \ln \frac{\mathsf{SNR}}{L_t|\Omega_t|} + o(\ln \mathsf{SNR})$$

as $\mathsf{SNR} \to \infty$.

# APPENDIX II
## PROOF OF LEMMA 3.3

The $F_\epsilon(x)$ can be expressed as

$$F_\epsilon(x) = \frac{M_t \ln(2\pi L_t|\Omega_t|)}{\pi^2 \bar{G}(\epsilon)} \Big( \ln \frac{1-\epsilon}{\epsilon} - \ln \frac{1-x}{x} \Big)$$
$$+ o\Big( \frac{\ln(L_t|\Omega_t|)}{L_t|\Omega_t|} \Big)$$

Now, we have

$$\int_\epsilon^1 \log x \, dF_\epsilon(x) = -\frac{M_t \ln(2\pi L_t|\Omega_t|)}{2\pi^2 \bar{G}(\epsilon) \ln 2} \Big[ \ln^2 \epsilon$$
$$+ 2\mathrm{Li}_2(1-\epsilon) \Big] + o\Big( \frac{\ln(L_t|\Omega_t|)}{L_t|\Omega_t|} \Big)$$

which yields

$$C_{MD} \gtrsim L_t|\Omega_t| \log \frac{\mathsf{SNR}}{l^{\nu-1}e} + \frac{1}{\pi^2} M_t \ln(2\pi L_t|\Omega_t|)$$
$$\Big[ \log \frac{\mathsf{SNR}}{l^{\nu-1}e} \ln \frac{1-\epsilon}{\epsilon} - \log \epsilon \ln \epsilon - \frac{2}{\ln 2} \mathrm{Li}_2(1-\epsilon) \Big]$$
$$+ o\big( \ln(L_t|\Omega_t|) \big)$$

as $L_t|\Omega_t| \to \infty$, for all $\epsilon \in (0,1)$. Now, we pick

$$\epsilon = \Big( \sqrt{\frac{\mathsf{SNR}}{l^{\nu-1}e}} \Big)^{-1} \tag{53}$$

and complete the proof.

# APPENDIX III
## PROOF OF LEMMA 3.4

We have

$$C_{MD} \leq \int_0^{1-\varepsilon} \log\Big(1 + \frac{\mathsf{SNR}}{l^{\nu-1}} x\Big) dG(x) + o\big(\ln(L_t|\Omega_t|)\big)$$
$$= \frac{1}{\pi^2 \ln 2} M_t \ln(2\pi L_t|\Omega_t|) \int_0^{1-\varepsilon} \frac{1}{x} \ln\Big(1 + \frac{\mathsf{SNR}}{l^{\nu-1}} x\Big)$$
$$+ \frac{1}{1-x} \ln\Big(1 + \frac{\mathsf{SNR}}{l^{\nu-1}} x\Big) dx + o\big(\ln(L_t|\Omega_t|)\big)$$

The first integral is

$$-\mathrm{Li}_2\Big( -\frac{\mathsf{SNR}}{l^{\nu-1}}(1-\varepsilon) \Big)$$

and the second integral is

$$\frac{\pi^2 L_t|\Omega_t|}{M_t \ln(2\pi L_t|\Omega_t|)} \ln\Big(1 + \frac{\mathsf{SNR}}{l^{\nu-1}}(1-\varepsilon)\Big)$$
$$- \ln\Big(1 + \frac{\mathsf{SNR}}{l^{\nu-1}}(1-\varepsilon)\Big) \ln \frac{\mathsf{SNR}/l^{\nu-1}(1-\varepsilon)}{1 + \mathsf{SNR}/l^{\nu-1}}$$
$$- \mathrm{Li}_2\Big( \frac{1 + \mathsf{SNR}/l^{\nu-1}(1-\varepsilon)}{1 + \mathsf{SNR}/l^{\nu-1}} \Big) + \mathrm{Li}_2\Big( \frac{1}{1 + \mathsf{SNR}/l^{\nu-1}} \Big)$$

As $\varepsilon$ approaches 0 for large $L_t|\Omega_t|$ and

$$\lim_{\mathsf{SNR} \to \infty} \frac{-\mathrm{Li}_2(-\mathsf{SNR}/l^{\nu-1})}{\ln^2(\mathsf{SNR}/l^{\nu-1})} = \frac{1}{2}$$

the upper-bound can be expressed as

$$C_{MD} \leq \Big[ L_t|\Omega_t| + M_t \ln(2\pi L_t|\Omega_t|) f_3(\mathsf{SNR}) \Big]$$
$$\log\Big(1 + \frac{\mathsf{SNR}}{l^{\nu-1}}\Big) + o\big(\ln(L_t|\Omega_t|)\big)$$

as $L_t|\Omega_t| \to \infty$, where

$$f_3(\mathsf{SNR}) = \frac{1}{2\pi^2} \ln \frac{\mathsf{SNR}}{l^{\nu-1}} + o(\ln \mathsf{SNR})$$

as $\mathsf{SNR} \to \infty$.

# APPENDIX IV
## PROOF OF THEOREM 4.2

The channel matrix for the single-bounce diffuse channel is block diagonal and each diagonal sub-block is an i.i.d. fading channel by itself. Suppose $d_i(r)$ satisfy

$$\lim_{\mathsf{SNR} \to \infty} \frac{\log P\big[\det(\mathbf{I} + \mathsf{SNR}\mathbf{H}_i^\dagger \mathbf{H}_i) < \mathsf{SNR}^r\big]}{\log \mathsf{SNR}} = -d_i(r)$$

for $i = 1, \cdots, M_t$. We follow the notation in [15] and use the symbol $\doteq$ to denote

$$\lim_{\mathsf{SNR} \to \infty} \frac{\log g(\mathsf{SNR})}{\log_2 \mathsf{SNR}} = b \iff g(\mathsf{SNR}) \doteq \mathsf{SNR}^b$$

Then, $d_i(r)$ satisfies

$$P\big[\det(\mathbf{I} + \mathsf{SNR}\mathbf{H}_i^\dagger \mathbf{H}_i) < \mathsf{SNR}^r\big] \doteq \mathsf{SNR}^{-d_i(r)}$$

Let $\mathsf{SNR}^{\theta_i} = \det(\mathbf{I} + \mathsf{SNR}\mathbf{H}_i^\dagger \mathbf{H}_i)$. The cdf of $\theta_i$ is

$$F_{\theta_i}(\theta) = P(\theta_i < \theta) \doteq \mathsf{SNR}^{-d_i(\theta)}$$

and thus, its pdf is

$$f_{\theta_i}(\theta) \doteq \frac{d}{d\theta} \mathsf{SNR}^{-d_i(\theta)}$$
$$= \mathsf{SNR}^{-d_i(\theta)} \ln \mathsf{SNR} \frac{d}{d\theta} d_i(\theta)$$
$$\doteq \mathsf{SNR}^{-d_i(\theta)}$$

ignoring the sign. Since the sub-blocks are independent, so

$$P\left[ \prod_{i=1}^{M_t} \det\left(\mathbf{I} + \mathsf{SNR}\mathbf{H}_i^\dagger \mathbf{H}_i\right) < \mathsf{SNR}^r \right]$$
$$= P\left( \sum_{i=1}^{M_t} \theta_i < r \right)$$
$$= (F_{\theta_1} * f_{\theta_2} * \cdots * f_{\theta_{M_t}})(r)$$
$$\doteq \mathsf{SNR}^{-d_{SD}(r)}$$

where

$$d_{SD}(r) = (d_1 \oplus d_2 \oplus \cdots \oplus d_{M_t})(r)$$

Now, we will show that $d_{SD}(r)$ is obtained by putting end-to-end the different linear pieces in $d_i(r)$'s, sorted by increasing slopes (or equivalently, decreasing negative slopes). It is sufficient to show that it holds for $M_t = 2$. Let $\tilde{d}(r)$ denote the claimed curve, and the slopes of $d_1(r)$ and $d_2(r)$ be $0 \geq s_1 \geq s_2 \geq \cdots \geq s_L$, with the corresponding length of projection onto the horizontal axis being $\alpha_1, \alpha_2, \cdots, \alpha_L$ where $L = \min\{L_t|\Omega_{t,1}|, L_r|\Omega_{r,1}|\} + \min\{L_t|\Omega_{t,2}|, L_r|\Omega_{r,2}|\}$. Furthermore, let $\mathcal{S}_n$ be the set of index of slopes belonging to $d_n(r)$, for $n = 1, 2$. Then, for $r \in \left[ L - \sum_{i=1}^{l} \alpha_i, L - \sum_{i=1}^{l-1} \alpha_i \right]$, the claimed curve is given by

$$\tilde{d}(r) = -\sum_{i=1}^{l-1} s_i \alpha_i - s_l \left( L - \sum_{i=1}^{l-1} \alpha_i - r \right)$$

Assume without loss of generality, $l \in \mathcal{S}_2$. We will show that when $r = L - \sum_{i=1}^{l-1} \alpha_i - \Delta$ for some $\Delta \in [0, \alpha_l)$,

$$d_1(u) + d_2(r-u) \geq d_1(a) + d_2(b), \quad \forall u \in [0, r]$$

where

$$a = \min\{L_t|\Omega_{t,1}|, L_r|\Omega_{r,1}|\} - \sum_{\substack{1 \leq i \leq l-1 \\ i \in \mathcal{S}_1}} \alpha_i$$
$$b = \min\{L_t|\Omega_{t,2}|, L_r|\Omega_{r,2}|\} - \sum_{\substack{1 \leq i \leq l-1 \\ i \in \mathcal{S}_2}} \alpha_i - \Delta$$

As $d_n(r)$'s are decreasing and piecewise linear, when $u \leq a$,

$$d_1(u) - d_1(a) \geq -s_l(a - u)$$

Note that $a + b = r$ and hence $r - u \geq b$. Thus,

$$d_2(b) - d_2(r-u) \leq -s_l(r - u - b) = -s_l(a - u)$$

Combining both inequalities gives the desired result. Similarly, when $u > a$,

$$d_1(a) - d_1(u) \leq -s_l(u - a)$$
$$d_2(r-u) - d_2(b) \geq -s_l(b - r + u) = -s_l(u - a)$$

Combining them gives the desired result as well. Furthermore, we have

$$d_1(a) + d_2(b) = -\sum_{\substack{1 \leq i \leq l-1 \\ i \in \mathcal{S}_1}} s_i \alpha_i - \sum_{\substack{1 \leq i \leq l-1 \\ i \in \mathcal{S}_2}} s_i \alpha_i - s_l \Delta$$
$$= -\sum_{i=1}^{l-1} s_i \alpha_i - s_l \left( L - \sum_{i=1}^{l-1} \alpha_i - r \right)$$
$$= \tilde{d}(r)$$

This implies that $d_1(u) + d2(r-u) \geq \tilde{d}(r)$. Since $d_{SD}(r)$ is the infimum of the sum on the left over all $u$ from 0 to $r$, it must coincide with the claimed curve on the right.

## REFERENCES

[1] D. S. Shiu, G. J. Foschini, M. J. Gans, and J. M. Kahn, "Fading correlation and its effect on the capacity of multielement antenna systems," *IEEE Trans. Commun.*, vol. 48, pp. 502–513, Mar. 2000.

[2] H. Bölcskei, D. Gesbert, and A. J. Paulraj, "On the capacity of OFDM-based spatial multiplexing systems," *IEEE Trans. Commun.*, vol. 50, pp. 225–234, Feb. 2002.

[3] C. N. Chuah, D. Tse, J. M. Kahn, and R. A. Valenzuela, "Capacity scaling in MIMO wireless systems under correlated fading," *IEEE Trans. Inform. Theory*, vol. 48, no. 3, pp. 637–650, Mar. 2002.

[4] D. Gesbert, T. Ekman, and N. Christophersen, "Capacity limits of dense palm-sized MIMO arrays," in *Proc. IEEE Global Telecommun. Conf.*, vol. 2, Taipei, Taiwan, Nov. 2002, pp. 17–21.

[5] J. Salz and J. H. Winters, "Effect of fading correlation on adaptive arrays in digital mobile radio," *IEEE Trans. Veh. Technol.*, vol. 43, no. 4, pp. 1049–1057, Nov. 1994.

[6] G. G. Raleigh and J. M. Cioffi, "Spatio-temporal coding for wireless communication," *IEEE Trans. Commun.*, vol. 46, no. 3, pp. 357–366, Mar. 1998.

[7] A. M. Sayeed, "Deconstructing multi-antenna fading channels," *IEEE Trans. Signal Processing*, vol. 50, pp. 2563–2579, Oct. 2002.

[8] T. S. Pollock, T. D. Abhayapala, and R. A. Kennedy, "Antenna saturation effects on MIMO capacity," in *Proc. IEEE Int. Conf. Commun.*, vol. 3, Anchorage, AK, May 2003, pp. 2301–2305.

[9] M. Debbah and R. Müller, "MIMO Channel Modeling and the Principle of Maximum Entropy," in *IEEE Trans. Inform. Theory*, vol. 51, no. 5, pp. 1667–1690, May 2005.

[10] R. R. Müller, "A random matrix model of communication via antenna arrays," *IEEE Trans. Inform. Theory*, vol. 48, no. 9, pp. 2495–2406, Sept. 2002.

[11] A. S. Y. Poon, R. W. Brodersen, and D. N. C. Tse, "Degrees of freedom in multiple-antenna channels: a signal space approach," *IEEE Trans. Inform. Theory*, vol. 51, no. 2, pp. 523–536, Feb. 2005.

[12] J. W. Wallace and M. A. Jensen, "Intrinsic capacity of the MIMO wireless channel," in *Proc. IEEE Veh. Technol. Conf.*, vol. 2, Vancouver, Canada, Sept. 2002, pp. 701–705.

[13] T. S. Rappaport, *Wireless Communications: Principle and Practice*, 2nd ed. Prentice Hall PTR, 2002.

[14] H. Özcelik and M. Herdin and W. Weichselberger and J. Wallace and E. Bonek, "Deficiencies of Kronecker MIMO radio channel model," *Electronics Letters*, vol. 39, no. 16, pp. 1209–1210, Aug. 2003.

[15] L. Zheng and D. N. C. Tse, "Diversity and multiplexing: a fundamental tradeoff in multiple antenna channels," *IEEE Trans. Inform. Theory*, vol. 49, pp. 1073–1096, May 2003.

[16] I. J. Gupta and A. A. Ksienski, "Effect of mutual coupling on the performance of adaptive arrays," *IEEE Trans. Antennas Propagat.*, vol. 31, no. 5, pp. 785–791, Sept. 1983.

[17] N. J. Kirsch and K. R. Dandekar, "Modeling effects of mutual coupling considered at both ends of a MIMO channel using computational electromagnetics," *Proc. IEEE Veh. Technol. Conf.*, vol. 6, pp. 4352–4355, 2004.

[18] D. F. Kelley and W. L. Stutzman, "Array antenna pattern modeling methods that include mutual coupling effects," *IEEE Trans. Antennas Propagat.*, vol. 41, no. 12, pp. 1625–1632, Dec. 1993.

[19] T. Su and H. Ling, "On modeling mutual coupling in antenna arrays using the coupling matrix," *Microwave and Optical Technol. Letters*, vol. 28, no. 4, pp. 231–237, Feb. 2001.

[20] L. Tsang, J. A. Kong, and K. H. Ding, *Scattering of Electromagnetic Waves: Theories and Applications*. Wiley, 2000.

[21] H. J. Landau and H. Widom, "Eigenvalue distribution of time and frequency limiting," *J. Math. Anal. and Appl.*, vol. 77, pp. 469–481, 1980.

[22] D. Slepian, "Some asymptotic expansions for prolate spheroidal wave functions," *J. of Mathematics and Physics*, vol. 44, pp. 99–140, 1965.

[23] R. G. Gallager, *Information Theory and Reliable Communication*. Wiley, 1968.

[24] V. L. Girko, *Theory of Random Determinants*. Norwell, MA: Kluwer, 1990.

[25] A. L. Moustakas, S. H. Simom, and A. M. Sengupta, "MIMO capacity through correlated channels in the presence of correlated interferers and noise: a (not so) large N analysis," *IEEE Trans. Infom. Theory*, vol. 49, no. 10, pp. 2545–2561, Oct. 2003.

[26] A. M. Tulino, A. Lozano, and S. Verdu, "Impact of antenna correlation on the capacity of multiantenna channels," *IEEE Trans. Infom. Theory*, vol. 51, no. 7, pp. 2491–2509, July 2005.

[27] D. Gesbert, "Multipath: Curse or blessing? a system performance analysis of MIMO wireless systems," in *Proc. of Intl. Zurich Seminar on Commun.*, 2004, pp. 14–17.

[28] J. L. Harris, "Diffraction and resolving power," *J. Opt. Soc. Am.*, vol. 54, no. 7, pp. 931–936, July 1964.

[29] G. T. di Francia, "Resolving power and information," *J. Opt. Soc. Am.*, vol. 45, no. 7, pp. 497–501, July 1955.

[30] D. Tse and P. Viswanath, *Fundamentals of Wireless Communication*. Cambridge University Press, 2005.

[31] Ö. Oyman and R. U. Nabar and H. Bölcskei and A. J. Paulraj, "Characterizing the statistical properties of mutual information in MIMO channels," *IEEE Trans. Signal Processing*, vol. 51, no. 11, pp. 2784–2795, Nov. 2003.

**Ada S. Y. Poon** (S'98–M'04) received the B.Eng and M.Phil. degrees in Electrical and Electronic Engineering from the University of Hong Kong in 1996 and 1997 respectively, and received the M.S. and Ph.D. degrees in Electrical Engineering and Computer Sciences from the University of California at Berkeley in 1999 and 2004 respectively.

From 2003 to 2005, she was a senior research scientist at Intel Corporation, Santa Clara. Currently, she is an assistant professor at the Department of Electrical and Computer Engineering in the University of Illinois at Urbana-Champaign. Her research interests are wireless communications, signal processing, VLSI circuits, and domain-specific hardware architecture.

**David N. C. Tse** (S'91–M'96) received the B.A.Sc. degree in systems design engineering from the University of Waterloo, Canada in 1889 and the M.S. and Ph.D. degrees in Electrical Engineering from the Massachusetts Institute of Technology, Cambridge in 1991 and 1994 respectively.

From 1994 to 1995, he was a postdoctoral member of technical staff at A.T. & T. Bell Laboratories. Since 1995, he has been at the Department of Electrical Engineering and Computer Sciences in the University of California at Berkeley, where he is currently a Professor. He received a 1967 NSERC 4-year graduate fellowship from the government of Canada in 1989, a NSF CAREER award in 1998, the Best Paper Awards at the Infocom 1998 and Infocom 2001 conferences, the Erlang Prize in 2000 from the INFORMS Applied Probability Society, the IEEE Communications and Information Theory Society Joint Paper Award in 2001, and the Information Theory Society Paper Award in 2003. He was the Technical Program co-chair of the International Symposium on Information Theory in 2004, and was an Associate Editor of the IEEE Transactions on Information Theory from 2001 to 2003. He is a coauthor, with Pramod Viswanath, of the text "Fundamentals of Wireless Communication". His research interests are in information theory, wireless communications and networking.

**Robert W. Brodersen** (M'76–SM'81–F'82) received the Bachelor of Science degrees in Electrical Engineering and Mathematics from California State Polytechnic University, Pomona, CA in 1966; the Engineers and Master of Science degrees from the Massachusetts Institute of Technology (MIT), Cambridge in 1968; and the Ph.D. degree in Engineering from MIT in 1972. He received the award Honor Doctor of Technology (Technologie Doctor Honoris Causa) from the University of Lund, Sweden in 1999.

From 1972-1976, he was a member of the Technical Staff, Central Research Laboratory, Texas Instruments, Dallas. In 1976, he joined the EECS faculty of the University of California at Berkeley, where he is now the John R. Whinnery Distinguished Professor in the Department of Electrical Engineering and Computer Sciences (EECS). His research is focused on new applications of integrated circuits in the area of low power design and wireless communications; and the algorithms, architectures and CAD tools necessary to support these activities. He is a member of the National Academy of Engineering.

Professor Brodersen has received a number of awards including: the IEEE Morris N. Liebmann Award in 1983 for pioneering work on switched-capacitor circuits; the Technical Achievement Award from the IEEE Circuits and Systems Society in 1986; the Technical Achievement Award from the Signal and Processing Society in 1991; the IEEE Solid-State Circuits Award in 1997 for contributions to the design of integrated circuits for signal processing systems; the Mobicom Award from ACM Sigmobile in 1998 for outstanding contribution to mobile computing; the IEEE CAS Golden Jubilee Medal in 2000 for outstanding contributions to the IEEE Circuit and Systems Society; and the IEEE Millenium Medal in 2000 for exceptional contributions towards advancing in various forms the Society's goals during the first 50 years of its history.

He received the best paper conference awards at Eascon in 1973, the International Solid-State Circuits Conferences in 1975, and the European Solid-State Circuits in 1978. In 1979, he received the W.G. Baker Award for the outstanding paper in the IEEE Journals and Transactions. In 1985, he received the best paper award in the Transactions on CAD. In 1992, he received the best tutorial paper of the IEEE Communications Society. In 2001, he was awarded the Lewis Winner Award for outstanding paper at the IEEE International Solid-State Circuits Conference (ISSCC). In 2003, he was given an award from ISSCC for being one of the top ten contributors over the 50 years of that society.

He was in involved in the founding of Atheros Communications in 1998 and is a member of a number of Technical Advisory boards for companies in the area of wireless communications, CAD tools and integrated circuits.